ISSN 2664-4150 (Print) & ISSN 2664-794X (Online)
**South Asian Research Journal of Engineering and Technology**
*Abbreviated Key Title: South Asian Res J Eng Tech*

**| Volume-8 | Issue-5 | Nov-Dec- 2026 |** **DOI: https://doi.org/10.36346/sarjet.2026.v08i05.002**

**Original Research Article**

# Interference Suppression Capability of the MVDR Adaptive Beamformer for Smart Antenna Systems: Effect of the Number of Interfering Signals on Null Depth, SIR and SINR

Suhail Najm Shahab[1]*

[1]Department of Network and Computer Software Engineering Technology, Polytechnic College – Hawija, Northern Technical University, Kirkuk, Iraq

***Corresponding Author:** Suhail Najm Shahab
Department of Network and Computer Software Engineering Technology, Polytechnic College – Hawija, Northern Technical University, Kirkuk, Iraq

**Article History**
Received: 13.09.2026
Accepted: 06.11.2026
Published: 20.11.2026

**Abstract:** Co-channel interference limits the capacity and reliability of modern wireless and navigation systems, and adaptive beamforming with antenna arrays is widely used to suppress it. The minimum variance distortionless response (MVDR) beamformer is the standard solution, but the effect of a growing number of signals not of interest (SNOI) on a fixed array is seldom quantified in a controlled way. This study aimed to determine how the number of SNOI affects the null depth, output signal-to-interference ratio (SIR), output signal-to-interference-plus-noise ratio (SINR) and mainlobe accuracy of an MVDR beamformer. An 8-element uniform linear array was simulated with the desired user at 0°, an input SNR of 10 dB and 250 snapshots, while the number of SNOI was increased from 1 to 9 at different angles, including two seven-interferer layouts. The deepest null per scenario ranged from −54 to −70 dB, and the mainlobe stayed at 0 dB within 0.006 dB. The output SIR was 54–55 dB for one and two SNOI, decreased to 43–50 dB for three to seven, and dropped to about 22 dB for eight and nine SNOI. The output SINR stayed at 19.0 dB, the noise-limited value, up to seven SNOI and fell to 17.3 dB beyond that. These results are consistent with the $N - 1$ degrees of freedom of the array. An $N$-element MVDR beamformer can therefore be relied upon to suppress up to $N - 1$ interferers, which gives a practical rule for dimensioning smart antenna arrays.

**Keywords:** MVDR Beamformer, Adaptive Beamforming, Interference Suppression, Uniform Linear Array, Null Steering, Signals Not of Interest, SIR, SINR, Degrees of Freedom, Smart Antenna.

## INTRODUCTION

The rapid growth of wireless services and the move toward millimetre-wave and terahertz links in sixth-generation systems have made spatial processing with antenna arrays indispensable, because beamforming provides both the gain needed to compensate path loss at these frequencies [1], and the spatial selectivity needed to separate users. At the same time, interference has become a first-order design problem. Managing co-channel interference from neighbouring cells is reported to be more complex in OFDM than in CDMA [2], satellite uplinks are exposed to co-channel interference from dense terrestrial networks [3], and satellite-navigation receivers are vulnerable to intentional and unintentional radio-frequency interference because the received signals are extremely weak [4]. Adaptive arrays that steer deep nulls toward interference are an effective response; a null-steering antenna for high-precision positioning, for example, has been reported to provide a 30 dB jamming advantage over a conventional GNSS patch antenna [5].

Among adaptive beamformers, the minimum variance distortionless response (MVDR), or Capon, beamformer [6], minimizes the array output power subject to a unit-gain constraint in the look direction, so that interference and noise are suppressed while the desired signal is preserved [7, 8]. It maximizes the output SINR when the interference-plus-noise

**Copyright © 2026 The Author(s):** This is an open-access article distributed under the terms of the Creative Commons Attribution **4.0 International License (CC BY-NC 4.0)** which permits unrestricted use, distribution, and reproduction in any medium for non-commercial use provided the original author and source are credited.

covariance matrix and the steering vector are known exactly [7]. In practice the covariance matrix is estimated from a finite number of snapshots, and the classical result is that sample matrix inversion needs a number of snapshots of the order of twice the number of array elements to approach the optimum performance [9].

Much of the recent MVDR literature addresses the sensitivity of the Capon beamformer to covariance and steering-vector errors. These errors sharply reduce the output SINR [10, 11], and can cause cancellation of the desired signal when it is present in the training data [12]. Remedies include diagonal loading with interference-plus-noise covariance reconstruction [13], reduced-dimension robust Capon beamforming based on Krylov subspaces [12], and generalized linear combination with adaptive loading, which was reported to reach near-optimal SINR with only 100 snapshots under steering-vector mismatch [14].

A second line of work concerns the degrees of freedom (DoF) that an array can spend on interference. For an MVDR beamformer facing D discrete interferers, the optimum processor operates in an interference subspace of dimension D + 1, which must be smaller than the number of array elements [15]. Allocating DoF between adaptive nulling and white-noise gain is a recognised trade-off: constraining every notch to be of second order, as is done to suppress moving interferers, consumes DoF that would otherwise reduce the white-noise sensitivity [16]. Other approaches enlarge the DoF themselves. Coprime and sparse arrays offer higher DoF and larger apertures than a uniform array with the same number of sensors, although holes in the difference coarray degrade adaptive beamforming unless the coarray is interpolated [17–19], and movable antennas add element position as a further DoF, enabling null steering toward all undesired directions under a sufficient number of antennas [20].

Learning-based and optimization-based methods have also been proposed. Convolutional and recurrent networks have been trained to estimate near-optimal weight vectors, in one case without knowledge of the direction of arrival of the desired signal and with as few as 400 snapshots [21], in another by combining a convolutional network with a bidirectional long short-term memory network [22], and by training a recurrent network on null-steering weights of a realistic microstrip array with mutual coupling [23]. A genetic algorithm combined with Schelkunoff nulling has been used for fast beam steering and null placement in a circular array [24], and adapting only part of the elements has been shown to give deep nulls with short convergence time [25]. Beyond radio frequencies, the same spatial filtering principle is applied in microphone arrays, where null broadening is used to overcome the bearing error between an interferer and its null [26].

Despite this progress, to the best of the author's knowledge the way in which the output SIR, SINR and null depth of the standard MVDR beamformer change as the number of interfering signals is increased on a fixed array, up to and beyond the DoF limit, is rarely isolated in a controlled study. Earlier work by the author examined MVDR performance for linear arrays as the noise variance and the number of interference sources were varied [27], and as the number of elements, element spacing, number of interference sources, noise power and number of snapshots were varied [28]. The present study fixes all other parameters and varies only the number of SNOI, so that its effect can be attributed unambiguously.

The objective of this study was therefore to quantify, by simulation, how the number of SNOI, from one to nine, influences the null depth, output SIR, output SINR and mainlobe accuracy of an MVDR beamformer applied to an 8-element uniform linear array (ULA), and to relate the observed behaviour to the DoF of the array. The novelty of the work lies in (i) a controlled sweep through and beyond the $N - 1$ limit with all other parameters fixed, (ii) the joint reporting of null depth, SIR, SINR, mainlobe accuracy and beamformer weights for every scenario, and (iii) the comparison of two different seven-interferer layouts to show the influence of angular geometry. The scope is limited to narrowband, far-field sources and an ideal array without steering-vector errors or mutual coupling.

## MATERIALS AND METHODS

A uniform linear array of $N = 8$ isotropic elements with an inter-element spacing of $d = \lambda/2$ was considered. A narrowband desired signal arriving from $\theta_s = 0°$ and $K$ signals not of interest (SNOI) arriving from $\theta_k$ ($k = 1, \ldots, K$) were modelled as uncorrelated far-field plane waves in additive white Gaussian noise. The snapshot vector received by the array is

$$\mathbf{x}(t) = \mathbf{a}(\theta_s)\, s(t) + \sum_{k=1}^{K} \mathbf{a}(\theta_k)\, i_k(t) + \mathbf{n}(t) \quad (1)$$

where $s(t)$ and $i_k(t)$ are the desired and interfering signals, $n(t)$ is the noise vector, and the steering vector is

$$\mathbf{a}(\theta) = \left[1,\ e^{j2\pi\frac{d}{\lambda}\sin\theta},\ \ldots,\ e^{j2\pi(N-1)\frac{d}{\lambda}\sin\theta}\right]^{\mathrm{T}} \quad (2)$$

The input SNR, $P_s/P_n$, was 10 dB and each SNOI was assigned the same power as the desired signal ($P_i = P_s$). The covariance matrix of the received data was estimated from $n_s = 250$ snapshots as

$$\hat{\mathbf{R}} = \frac{1}{n_s}\sum_{m=1}^{n_s} \mathbf{x}(m)\,\mathbf{x}^{\mathrm{H}}(m) \quad (3)$$

Because $n_s$ is about 31 times the number of elements and far exceeds the order of $2N = 16$ snapshots needed for the sample covariance matrix to approach the optimum [9], covariance estimation error was not expected to be the limiting factor. The MVDR weight vector minimizes the output power $\mathbf{w}^{\mathrm{H}}\,\hat{\mathbf{R}}\,\mathbf{w}$ subject to the distortionless constraint $\mathbf{w}^{\mathrm{H}}\,\mathbf{a}(\theta_s) = 1$ and is given by

$$\mathbf{w} = \frac{\hat{\mathbf{R}}^{-1}\mathbf{a}(\theta_s)}{\mathbf{a}^{\mathrm{H}}(\theta_s)\,\hat{\mathbf{R}}^{-1}\mathbf{a}(\theta_s)} \quad (4)$$

The following performance measures were evaluated for each scenario. The normalized beam pattern was computed as

$$P(\theta) = 20\log_{10}|\mathbf{w}^{\mathrm{H}}\mathbf{a}(\theta)| \quad \text{(dB)} \quad (5)$$

The deepest null was taken as the lowest value of $P(\theta)$ at the interferer directions, and the mainlobe accuracy as the deviation of the peak power from 0 dB and the angle at which the peak occurred. The output SIR was obtained from

$$\mathrm{SIR}_{\mathrm{out}} = 10\log_{10}\frac{P_s|\mathbf{w}^{\mathrm{H}}\mathbf{a}(\theta_s)|^2}{\sum_{k=1}^{K} P_i\,|\mathbf{w}^{\mathrm{H}}\mathbf{a}(\theta_k)|^2} \quad (6)$$

and the output SINR from

$$\mathrm{SINR}_{\mathrm{out}} = 10\log_{10}\frac{P_s}{P_{i,\mathrm{out}} + P_n/N}, \qquad P_{i,\mathrm{out}} = \sum_{k=1}^{K} P_i\,|\mathbf{w}^{\mathrm{H}}\mathbf{a}(\theta_k)|^2 \quad (7)$$

Where the term $P_n/N$ is the output noise power that results when the white-noise gain of the beamformer equals the number of elements. The exact noise power at the output is $P_n\,\mathbf{w}^{\mathrm{H}}\,\mathbf{w}$, and the effect of this approximation was assessed using

$$\mathrm{SINR}_{\mathrm{out}}^{\mathrm{exact}} = 10\log_{10}\frac{P_s}{P_{i,\mathrm{out}} + P_n\,\mathbf{w}^{\mathrm{H}}\mathbf{w}} \quad (8)$$

The weight vector and the execution time of each run were also recorded. Ten scenarios were simulated (Table 1): $K = 1$ to 9, with SNOI directions added progressively, and an additional seven-SNOI layout with widely spread angles (−83°, −66°, −35°, −17°, 18°, 32° and 54°) to examine the influence of angular geometry at a fixed $K$.

## Results and Discussion

Table 1 summarizes the results of the ten scenarios and Fig. 1 shows the trends of the output SIR, SINR and deepest null level with the number of SNOI. Three regimes can be identified. For one and two SNOI the output SIR was 54.4 and 54.9 dB. For three to seven SNOI it decreased gradually from 49.6 dB ($K = 3$) to 43.4 dB ($K = 7$). When the number of SNOI reached eight and nine, the SIR collapsed to 22.2 dB in both cases, a reduction of about 21 dB with respect to seven SNOI. The output SINR followed a different pattern: it remained between 19.015 and 19.030 dB for one to seven SNOI and decreased to 17.34 and 17.32 dB only for eight and nine SNOI. The deepest null ranged from −54.4 to −70.1 dB and showed no systematic dependence on $K$ (Fig. 1b).

**Table 1: Performance of the MVDR beamformer versus the number of SNOI (8-element ULA, desired user at 0°, SNR = 10 dB, 250 snapshots)**

| *K* | SNOI directions (°) | Deepest null (dB) | SIR (dB) | SINR (dB) | Peak offset (dB / °) | Time (s) |
|---|---|---|---|---|---|---|
| 1 | 30 | −54.42 | 54.42 | 19.03 | $1.6\times10^{-4}$ / −1 | 0.748 |
| 2 | ±30 | −70.13 | 54.87 | 19.03 | 0.0053 / −1 | 0.913 |
| 3 | 15, ±30 | −61.35 | 49.58 | 19.03 | 0 / 0 | 0.645 |
| 4 | ±15, ±30 | −66.42 | 47.97 | 19.03 | 0 / 0 | 0.724 |
| 5 | ±15, ±30, 50 | −59.37 | 47.81 | 19.03 | 0 / 0 | 0.702 |
| 6 | ±15, ±30, ±50 | −65.10 | 47.16 | 19.02 | ≈0 / 0 | 0.740 |
| 7 | ±15, ±30, ±50, −83 | −58.12 | 43.39 | 19.02 | ≈0 / 0 | 0.700 |
| 8 | ±15, ±30, ±50, ±80 | −59.61 | 22.24 | 17.34 | 0 / 0 | 0.610 |
| 9 | ±15, ±30, ±50, ±80, 60 | −57.17 | 22.18 | 17.32 | 0 / 0 | 0.595 |
| 7b | −83, −66, −35, −17, 18, 32, 54 | −60.33 | 45.96 | 19.02 | 0 / 0 | 0.679 |

**Notes**: SIR and SINR are output values from Eqs. (6) and (7). Peak offset = deviation of the mainlobe peak power from 0 dB (dB) / angle of the peak (°). Time = execution time of a single run. 7b = dispersed seven-SNOI layout.

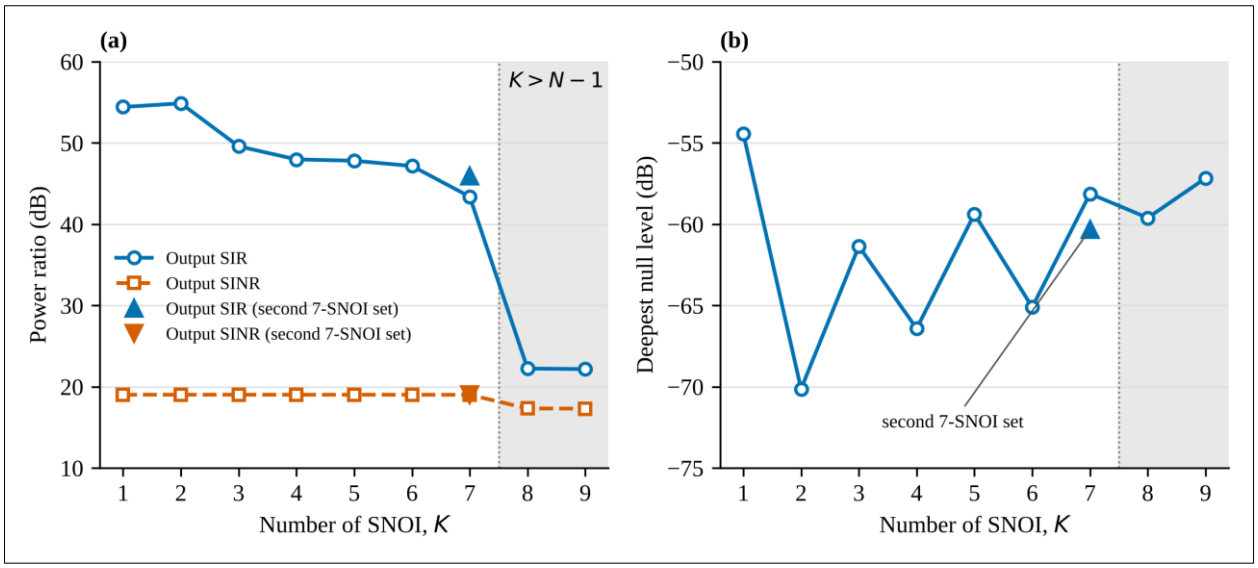



**Figure 1: (a) Output SIR and SINR and (b) deepest null level of the MVDR beamformer versus the number of SNOI (8-element ULA, SNR = 10 dB, 250 snapshots). Triangles: second seven-SNOI layout. Shaded region: $K > N - 1$.**

## Beam Patterns

The beam patterns confirm that the beamformer kept the mainlobe at 0° and placed nulls at the interferer directions. With one SNOI (Fig. 2a), a single deep null of about −54 dB was formed at 30°, whereas the other minima of the pattern were shallow (about −26 to −32 dB) and corresponded to ordinary sidelobe minima. With two SNOI at ±30° (Fig. 2b) the nulls reached about −55 dB at −30° and −70 dB at 30°. Adding interferers at 15° (Fig. 2c) and at ±15° (Fig. 2d) produced additional nulls at the edge of the mainlobe, close to the first null of the uniform-weight pattern of an 8-element, half-wavelength array (≈14.5°).

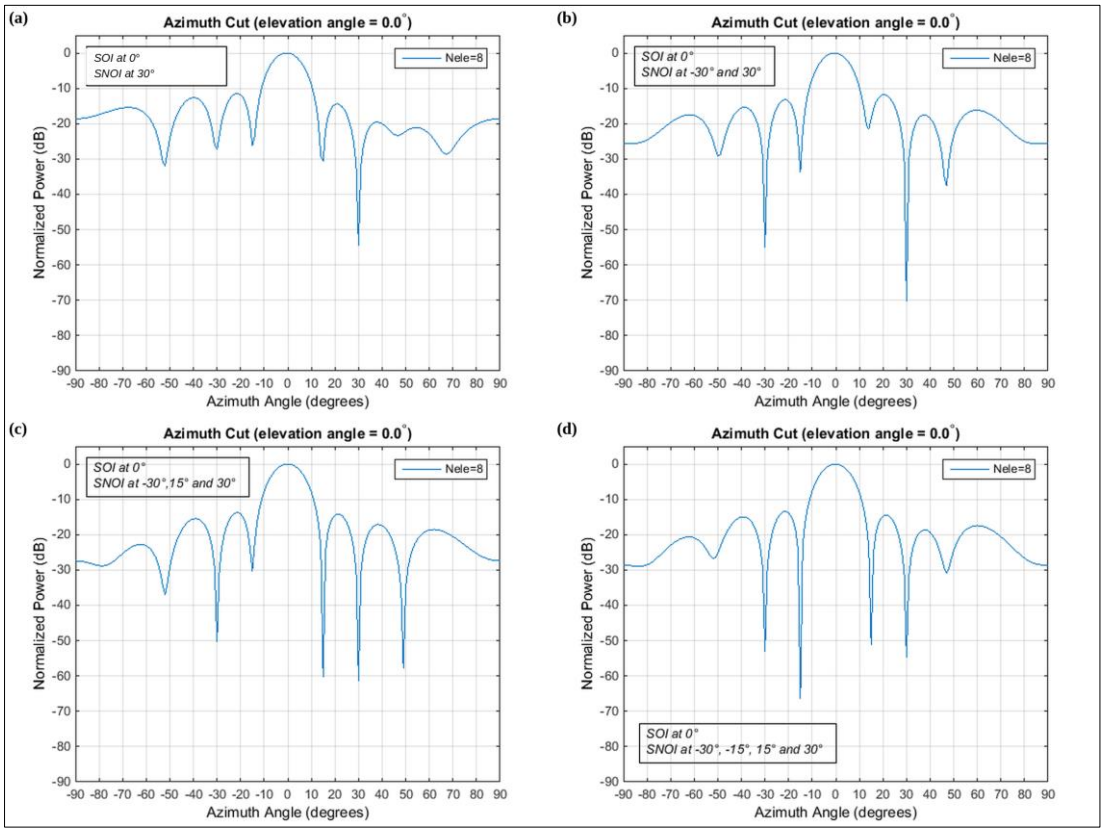



**Figure 2: Azimuth beam patterns of the MVDR beamformer for (a) $K = 1$ (30°), (b) $K = 2$ (±30°), (c) $K = 3$ (15°, ±30°) and (d) $K = 4$ (±15°, ±30°)**

For five to seven SNOI (Fig. 3) every interferer direction carried a distinct null; evaluating the pattern at the interferer directions from the tabulated weights gave null levels between about −49 and −59 dB for the seven-SNOI layout with ±15°, ±30°, ±50° and −83° (Fig. 3c), and between −49 and −61 dB for the dispersed layout (Fig. 3d).

With nine SNOI (Fig. 4) the pattern changed qualitatively. Although the deepest null was still −57.2 dB, the attenuation at individual interferer directions, computed from the tabulated weights, varied from about −25 to −57 dB, with the directions at 50°, 60° and −80° receiving only about −25 to −30 dB. Several interferers were thus no longer effectively nulled, which explains the drop in SIR to 22.2 dB.

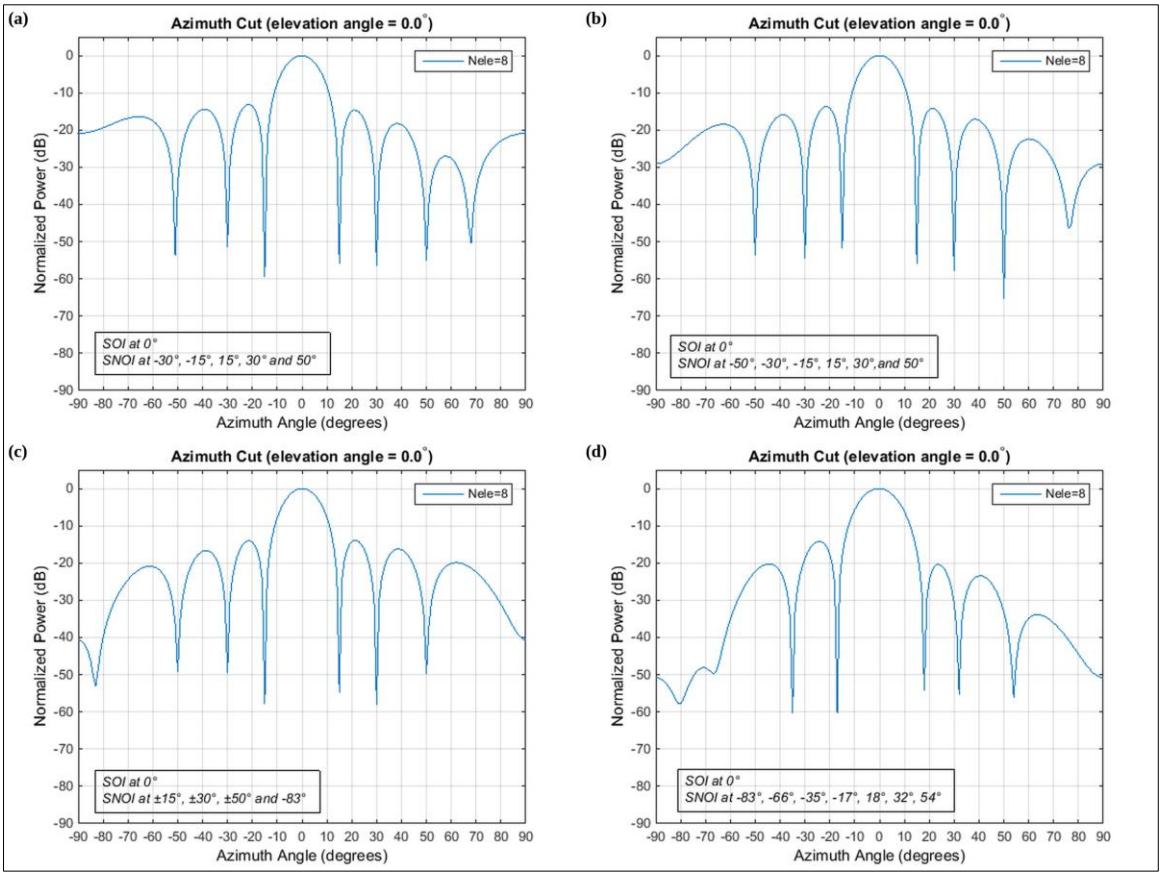



**Figure 3: Azimuth beam patterns for (a) $K = 5$ (±15°, ±30°, 50°), (b) $K = 6$ (±15°, ±30°, ±50°), (c) $K = 7$ (±15°, ±30°, ±50°, −83°) and (d) the dispersed seven-SNOI layout (−83°, −66°, −35°, −17°, 18°, 32°, 54°)**

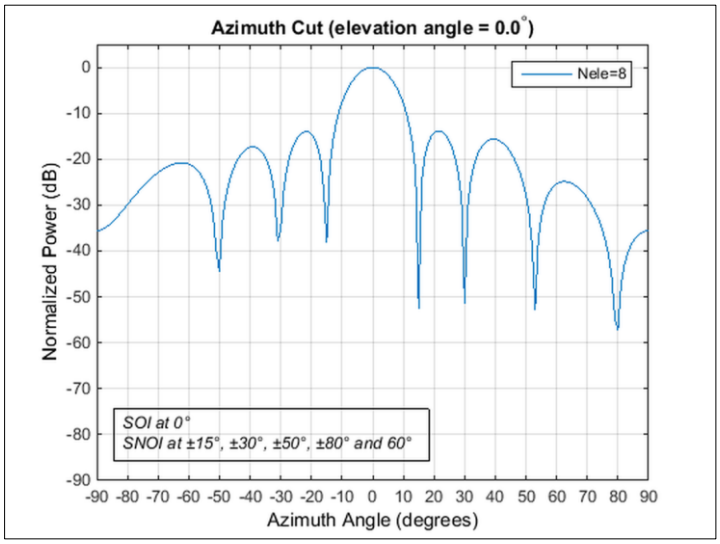



**Figure 4: Azimuth beam pattern for $K = 9$ (±15°, ±30°, ±50°, ±80°, 60°), exceeding the limit $N - 1 = 7$**

**Degrees of Freedom and the Output SIR**

The behaviour in Fig. 1a is consistent with the DoF of the array. With the unit-gain constraint in the look direction, an $N$-element linear array has $N - 1 = 7$ DoF available for interference rejection, so that up to seven interferers can be nulled independently. A related condition, namely that the interference subspace must have a dimension smaller than the number of elements, underlies the analysis of Singh *et al*., [15]. Because each SNOI in this study had a power 10 dB above the noise at the element level, the MVDR solution approximates a null-constrained design, and the SIR remained high as long as $K \leq 7$. For $K = 8$ and 9 the array can no longer place an independent null on every interferer; the beamformer can only minimize the total output power, and the residual interference rose to about −22 dB relative to the desired signal.

The gradual decrease of the SIR from 54.4 dB ($K = 1$) to 43.4 dB ($K = 7$), a reduction of 11.0 dB, has two causes. First, the output SIR is determined by the sum of the residuals left by all nulls, so that seven equal residuals would alone reduce the SIR by $10 \log_{10} 7 \approx 8.5$ dB with respect to a single null. Second, the remaining ≈2.6 dB is compatible with slightly shallower individual nulls (about −49 to −59 dB for $K = 7$) as DoF are consumed. The deepest null alone is therefore a poor indicator of overall interference rejection: at $K = 8$ and 9 it was still −59.6 and −57.2 dB, yet the SIR had fallen by about 21 dB. The SIR, which accumulates all residuals, is the more informative metric.

**Output SINR**

For $K \leq 7$ the output SINR was 19.015–19.030 dB, which equals the noise-limited value SNR + $10 \log_{10} N = 10 + 9.03 = 19.03$ dB to within 0.015 dB. The residual interference, 43–55 dB below the desired signal, was more than 24 dB below the output noise (−19.03 dB), so it had practically no effect on the SINR. For this reason the SINR is not a sensitive indicator of the number of SNOI as long as the DoF are not exhausted. Beyond the limit the SINR followed Eq. (7): for $K = 8$ the output noise ($10^{-1.903} = 0.0125$ of the desired signal power) and the residual interference ($10^{-2.224} = 0.0060$) add to approximately 0.0185, which corresponds to 17.34 dB, as listed in Table 1; the same calculation gives 17.32 dB for $K = 9$.

**Influence of Angular Geometry**

The two seven-SNOI layouts gave different results although $K$ was the same. The dispersed layout produced a 2.6 dB higher SIR (45.96 versus 43.39 dB) and a deepest null of −60.3 dB versus −58.1 dB, with practically the same SINR (19.022 versus 19.015 dB). The weights differed markedly: for all other scenarios the weight magnitudes lay between 0.109 and 0.147, close to the uniform value $1/N = 0.125$, whereas for the dispersed layout they ranged from 0.067 to 0.158 with strongly reduced edge-element weights. A possible explanation is that interferers at ±15° lie close to the first null of the quiescent pattern, so that the corresponding nulls can be formed with little change of the uniform weights, while the dispersed layout requires a stronger weight taper that, in turn, increases the noise gain. This interpretation was not tested further and deserves a dedicated study of angular separation.

**Mainlobe Accuracy and Weights**

The mainlobe peak coincided with the desired direction (0°) for all scenarios except $K = 1$ and 2, in which the peak was found at −1°. The corresponding power deviations were only $1.6 \times 10^{-4}$ dB and 0.0053 dB, so the desired signal was preserved in practice, as required by the distortionless constraint. The sum of the weights was 1.000 ± 0.0002 in all scenarios, which confirms that the constraint was satisfied. The squared weight norm $\mathbf{w}^{H}\,\mathbf{w}$ was between 0.1255 and 0.1289 for all scenarios except the dispersed layout (0.1349), compared with 0.125 for uniform weights (Table 2). Re-evaluating the SINR with the exact noise gain (Eq. 8) therefore lowered it by only 0.02–0.13 dB for the scenarios with $K \leq 7$ in the first layout, 0.03 dB for $K = 8$ and 9, and 0.33 dB for the dispersed layout, so the approximation $P_n/N$ in Eq. (7) does not alter any conclusion.

**Table 2: Weight-vector statistics and effect of the exact noise gain on the output SINR**

| *K* | Weight magnitude range | $\mathbf{w}^{H}\mathbf{w}$ | WNG (dB) | SINR, Eq. (7) (dB) | SINR, exact (dB) | Difference (dB) |
|---|---|---|---|---|---|---|
| 1 | 0.113–0.143 | 0.1289 | 8.90 | 19.03 | 18.90 | 0.13 |
| 2 | 0.110–0.138 | 0.1272 | 8.96 | 19.03 | 18.95 | 0.07 |
| 3 | 0.112–0.143 | 0.1261 | 8.99 | 19.03 | 18.99 | 0.04 |
| 4 | 0.111–0.147 | 0.1263 | 8.99 | 19.03 | 18.98 | 0.04 |
| 5 | 0.115–0.137 | 0.1266 | 8.97 | 19.03 | 18.97 | 0.06 |
| 6 | 0.113–0.136 | 0.1256 | 9.01 | 19.02 | 19.00 | 0.02 |
| 7 | 0.114–0.136 | 0.1255 | 9.01 | 19.02 | 19.00 | 0.02 |
| 8 | 0.109–0.138 | 0.1261 | 8.99 | 17.34 | 17.31 | 0.03 |
| 9 | 0.109–0.137 | 0.1261 | 8.99 | 17.32 | 17.29 | 0.03 |
| 7b | 0.067–0.158 | 0.1349 | 8.70 | 19.02 | 18.69 | 0.33 |

**Notes**: Statistics were computed from the weight vectors listed in the results (four decimals). SINR (Eq. 7) uses $P_n/N$; SINR (exact) uses $P_n\,\mathbf{w}^{H}\,\mathbf{w}$ (Eq. 8). WNG = white-noise gain = $-10 \log_{10} (\mathbf{w}^{H}\,\mathbf{w})$. 7b = dispersed seven-SNOI layout.

**Execution Time**

The recorded execution times ranged from 0.595 to 0.913 s without any systematic dependence on $K$ (Table 1). This is expected because the computational cost of the MVDR beamformer is dominated by the estimation and inversion of the 8 × 8 covariance matrix, which does not depend on the number of interferers. Since each time was measured in a single run, the differences between scenarios should be attributed to measurement variability and not to the beamformer.

**Implications and Comparison with Earlier Work**

The results provide a simple design rule: an $N$-element MVDR beamformer can suppress up to $N - 1$ interferers, and the SIR margin shrinks as $K$ approaches this limit, so that arrays should be dimensioned with $N \geq K + 1$ plus a margin for the expected angular geometry. This is consistent with the earlier observation that the SINR of a linear-array MVDR beamformer depends on the number of interference sources [27], and it clarifies that, when the noise level and the number of snapshots are fixed, the dependence appears in the SIR and null depth long before it appears in the SINR, which changes only once the DoF are exhausted. The number of snapshots used here (250, i.e. 31$N$) exceeds the order of 2$N$ required for convergence of the sample covariance matrix [9], so the collapse at $K = 8$ is due to the lack of DoF and not to finite-sample covariance error. Because learning-based [21-23], and optimization-based [24, 25], methods that set the array weights also form linear combinations of the $N$ element outputs, they would be expected to remain bound by the same $N - 1$ limit unless the array geometry itself is changed; coprime and sparse arrays [17–19], or movable antennas [20], are the routes by which the limit can be extended.

**Limitations**

The conclusions are limited to a single array size ($N = 8$, half-wavelength spacing), one noise level (SNR = 10 dB), one snapshot number (250), equal-power uncorrelated narrowband interferers, an ideal array without steering-vector error or mutual coupling, and a single realization of the snapshot matrix per scenario. Monte Carlo averaging over many realizations, variation of $N$ to verify that the collapse point follows $N - 1$, unequal interferer powers, steering-vector errors and mutual coupling, correlated or multipath sources, and a comparison with robust MVDR variants and sparse arrays are recommended for future work.

# CONCLUSION

The effect of the number of signals not of interest on the performance of an MVDR beamformer applied to an 8-element uniform linear array was investigated by simulation. The main findings were:

- The beamformer preserved the desired signal at 0° (peak power deviation below 0.006 dB) and formed deep nulls, with the deepest null of each scenario between −54 and −70 dB.
- The output SIR was 54.4–54.9 dB for one and two SNOI, 43.4–49.6 dB for three to seven SNOI, and about 22 dB for eight and nine SNOI.
- The output SINR was noise-limited at 19.0 dB up to seven SNOI and fell to 17.3 dB for eight and nine SNOI, so SIR and null level are more sensitive indicators than SINR below the DoF limit.
- The collapse of the SIR at eight SNOI is consistent with the $N - 1 = 7$ degrees of freedom of the array; an $N$-element MVDR beamformer can reliably suppress up to $N - 1$ interferers.
- The angular layout matters: a dispersed seven-SNOI layout gave a 2.6 dB higher SIR than the clustered layout.
- Future work should use Monte Carlo averaging, vary the array size, and include unequal interferer powers, steering-vector errors and mutual coupling.

# REFERENCES

1. Xue Q, Ji C, Ma S, Guo J, Xu Y, Chen Q, et al. A survey of beam management for mmWave and THz communications towards 6G. IEEE Commun Surv Tutor. 2024. doi:10.1109/COMST.2024.3361991.
2. Shivam Y, Prashant K, Ravi KS, Vivek R, Devasis P. A detail survey of channel access method for cognitive radio network (CRN) applications toward 4G. South Asian Res J Eng Tech. 2021;3(1):31-41. doi:10.36346/sarjet.2021.v03i01.005.
3. Zhang J, Zhang X, Sheng T, Lv Z, Yuan C, Zhou Z, et al. Database-guided local refinement and truncated power estimation for LEO uplink anti-interference beamforming. Sensors. 2026;26(11):3482. doi:10.3390/s26113482.
4. Lorraine KJS, Ramarakula M. A comprehensive survey on GNSS interferences and the application of neural networks for anti-jamming. IETE J Res. 2021. doi:10.1080/03772063.2021.1953407.
5. Pal A, Mehta A, Skippins A, Spicer P, Mirshekar-Syahkal D. Novel interference suppression null steering antenna system for high precision positioning. IEEE Access. 2020;8. doi:10.1109/ACCESS.2020.2988881.
6. Capon J. High-resolution frequency-wavenumber spectrum analysis. Proc IEEE. 1969;57(8):1408-1418. doi:10.1109/PROC.1969.7278.
7. Van Trees HL. Optimum Array Processing: Part IV of Detection, Estimation, and Modulation Theory. New York: Wiley; 2002. doi:10.1002/0471221104.

8. Godara LC. Application of antenna arrays to mobile communications, Part II: Beam-forming and direction-of-arrival considerations. Proc IEEE. 1997;85(8):1195-1245. doi:10.1109/5.622504.
9. Reed IS, Mallett JD, Brennan LE. Rapid convergence rate in adaptive arrays. IEEE Trans Aerosp Electron Syst. 1974;AES-10(6):853-863. doi:10.1109/TAES.1974.307893.
10. Meng W, Ke Y, Li J, Zheng C, Li X. Finite data performance analysis of one-bit MVDR and phase-only MVDR. Signal Process. 2021;108018. doi:10.1016/j.sigpro.2021.108018.
11. Cox H, Zeskind RM, Owen MM. Robust adaptive beamforming. IEEE Trans Acoust Speech Signal Process. 1987;35(10):1365-1376. doi:10.1109/TASSP.1987.1165054.
12. Wang X, Jiang X, Chen Y. An improved reduced-dimension robust Capon beamforming method using Krylov subspace techniques. Sensors. 2024;24(22):7152. doi:10.3390/s24227152.
13. Yang Y, Xu X, Yang H, Li W. Robust adaptive beamforming via covariance matrix reconstruction with diagonal loading on interference sources covariance matrix. Digit Signal Process. 2023;103977. doi:10.1016/j.dsp.2023.103977.
14. Gao Z, Zuo R, Huang P, Xu W, Tan W, Wu Z. Robust adaptive beamforming algorithm based on improved generalized linear combination. Sensors. 2026;26(11):3385. doi:10.3390/s26113385.
15. Singh S, Singh SV, Yadav D, Suman SK, Lakshminarayanan B, Singh G. Discrete interferences optimum beamformer in correlated signal and interfering noise. Int J Electr Comput Eng. 2022;12(2):1732-1743. doi:10.11591/ijece.v12i2.pp1732-1743.
16. Erdim S, et al. Mitigating multiple moving interferers with the hybrid double zero MVDR beamformer. IEEE Access. 2024. doi:10.1109/ACCESS.2024.3437749.
17. Zheng Z, Yang T, Wang WQ, Zhang S. Robust adaptive beamforming via coprime coarray interpolation. Signal Process. 2020. doi:10.1016/j.sigpro.2019.107382.
18. Zheng Z, Fu Y, Wang WQ. Sparse array beamforming design for coherently distributed sources. IEEE Trans Antennas Propag. 2021. doi:10.1109/TAP.2020.3028190.
19. Chen S, Wu X, Li S, Deng W, Zhang X. Efficient and robust adaptive beamforming based on coprime array interpolation. Remote Sens. 2024;16(15):2792. doi:10.3390/rs16152792.
20. Zhu L, Ma W, Zhang R. Movable-antenna array enhanced beamforming: achieving full array gain with null steering. IEEE Commun Lett. 2023. doi:10.1109/LCOMM.2023.3323656.
21. Ramezanpour P, Rezaei MJ, Mosavi MR. Deep-learning-based beamforming for rejecting interferences. IET Signal Process. 2020. doi:10.1049/iet-spr.2019.0495.
22. Ramezanpour P, Mosavi MR. Two-stage beamforming for rejecting interferences using deep neural networks. IEEE Syst J. 2021. doi:10.1109/JSYST.2020.3034957.
23. Mallioras I, Zaharis ZD, Lazaridis PI, Pantelopoulos S. A novel realistic approach of adaptive beamforming based on deep neural networks. IEEE Trans Antennas Propag. 2022. doi:10.1109/TAP.2022.3168708.
24. Hamza A, Attia H. Fast beam steering and null placement in an adaptive circular antenna array. IEEE Antennas Wirel Propag Lett. 2020. doi:10.1109/LAWP.2020.3009905.
25. Mohammed JR. Interference mitigation in the wireless communication systems using adaptive filters. IOP Conf Ser Mater Sci Eng. 2021;1152:012001. doi:10.1088/1757-899X/1152/1/012001.
26. Wu BH. Application of microphone arrays to interference cancellation by using null broadening beamforming. Sens Actuators A Phys. 2023. doi:10.1016/j.sna.2022.114059.
27. Shahab SN, Zainun AR, Mohd II, Noordin NH. The impact of noise label on beampattern and SINR of MVDR beamformer. Int J Comput Commun Instrum Eng. 2016;3(1):89-95. doi:10.15242/IJCCIE.ER0116122.
28. Shahab SN, Zainun AR, Ali HA, Hojabri M, Noordin NH. MVDR algorithm based linear antenna array performance assessment for adaptive beamforming application. J Eng Sci Technol. 2017;12(5):1366-1385.